NREL
NATIONAL RENEWABLE ENERGY LABORATORY

Influence of Damp Heat on the Electrical, Optical, and Morphological Properties of Encapsulated $CuInGaSe_2$ Devices

Preprint

R. Sundaramoorthy, F.J. Pern, G. Teeter, J.V. Li, M. Young, D. Kuciauskas, N. Call, F. Yan, B. To, S. Johnston, R. Noufi, and T.A. Gessert

Presented at the 37th IEEE Photovoltaic Specialists Conference (PVSC 37)
Seattle, Washington
June 19-24, 2011

Conference Paper
NREL/CP-5200-50841
August 2011

Contract No. DE-AC36-08GO28308

NOTICE

Available electronically at http://www.osti.gov/bridge

Available for a processing fee to U.S. Department of Energy
and its contractors, in paper, from:

U.S. Department of Energy
Office of Scientific and Technical Information

P.O. Box 62
Oak Ridge, TN 37831-0062
phone: 865.576.8401
fax: 865.576.5728
email: mailto:reports@adonis.osti.gov

Available for sale to the public, in paper, from:

U.S. Department of Commerce
National Technical Information Service
5285 Port Royal Road
Springfield, VA 22161
phone: 800.553.6847
fax: 703.605.6900
email: orders@ntis.fedworld.gov
online ordering: http://www.ntis.gov/help/ordermethods.aspx

Cover Photos: (left to right) PIX 16416, PIX 17423, PIX 16560, PIX 17613, PIX 17436, PIX 17721

Printed on paper containing at least 50% wastepaper, including 10% post consumer waste.

INFLUENCE OF DAMP HEAT ON THE ELECTRICAL, OPTICAL, AND MORPHOLOGICAL PROPERTIES OF ENCAPSULATED $CuInGaSe_2$ DEVICES

R. Sundaramoorthy, F.J. Pern, G. Teeter, Jian V. Li, M. Young, D. Kuciauskas, N. Call, F. Yan, B. To
S. Johnston, R. Noufi and T. A. Gessert
National Center for Photovoltaics, National Renewable Energy Laboratory, 1617 Cole Blvd., Golden, CO 80401, USA

ABSTRACT

$CuInGaSe_2$ (CIGS) devices, encapsulated with different backsheets having different water vapor transmission rates (WVTR), were exposed to damp heat (DH) at 85°C and 85% relative humidity (RH) and characterized periodically to understand junction degradation induced by moisture ingress. Performance degradation of the devices was primarily driven by an increase in series resistance within first 50 h of exposure, resulting in a decrease in fill factor and, accompanied loss in carrier concentration and widening of depletion width. Surface analysis of the devices after 700-h DH exposure showed the formation of $Zn(OH)_2$ from hydrolysis of the Al-doped ZnO (AZO) window layer by the moisture, which was detrimental to the collection of minority carriers. Minority carrier lifetimes observed for the CIGS devices using time resolved photoluminescence (TRPL) remained relatively long after DH exposure. By etching the DH-exposed devices and re-fabricating with new component layers, the performance of reworked devices improved significantly, further indicating that DH-induced degradation of the AZO layer and/or the CdS buffer was the primary performance-degrading factor.

INTRODUCTION

Thin-film CIGS photovoltaics (PV) has reached a point at which its large-scale production is undertaken by several companies. Not only is a PV module's power output essential, but its long-term performance reliability is also a deciding factor for the establishment of the technology in the PV market. The reliability of a module depends on many factors [1-2], namely environmental elements such as temperature, humidity, UV exposure, rain, hail, etc. In particular, the combination of temperature and humidity plays a very crucial role in the stability of the components of a PV module. To understand the collective effect of the individual layers on the degradation of the junction, we studied the stability of CIGS solar cells encapsulated with different backsheets under DH conditions using various characterization techniques.

EXPERIMENTAL

Sample Preparations. CIGS devices were fabricated using NREL's three-stage process on Mo-sputtered soda lime glass (SLG) substrate followed by a chemical-bath-deposited CdS layer and a bi-layer of intrinsic ZnO and ZnO:Al as the buffer and conducting layers, respectively. Ni/Al trident grids were deposited as the front contacts. The devices were electrically isolated by a photolithographic process. The six individual coupons cut from the 3" by 3" substrate [3] were encapsulated in an Al frame with a borosilicate float glass on the top and a backsheet, such as Tefzel, TPT, TPAT or glass, at the bottom for moisture ingress control, as described previously in ref. [4]. Their respective WVTR are 5.5, 4, 0.001, and ~$1*10^{-5}$ gm/m^2-day. Figure 1 shows an example of a cell coupon before and after encapsulation.

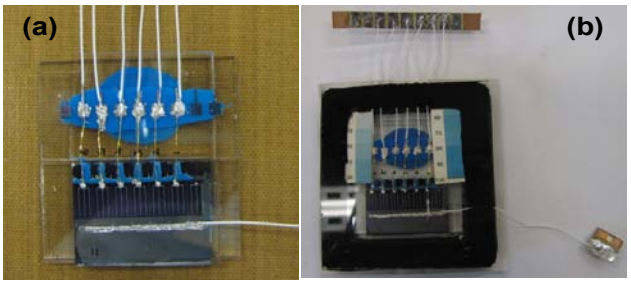

Figure 1 CIGS cell coupon (a) before and (b) after encapsulation.

DH Exposure and Device Characterization. Baseline optical (UV-Vis), electrical (J-V, C-V), and structural (x-ray diffraction) measurements were performed on all of the samples before encapsulation and exposure to DH conditions at 85° C and 85% RH in an ESPEC environmental chamber. The CIGS samples were measured for their electrical performance using a solar simulator at 25°C at AM1.5 conditions and also in the dark every one or two hours. Once the devices were below 10% of the initial performance, the backsheet was removed and the devices were further analyzed using x-ray photo-electron spectroscopy (XPS) for chemical shifts in the core levels. The Al K_α line (1486.6eV) was used as the x-ray source to record the XPS survey spectra and high resolution core level spectra of the following elements, Zn 2p, O 1s, C 1s, and Na 1s. Secondary ion mass spectroscopy (SIMS) analysis was conducted to track possible mobile ions. Photoluminescence (PL) imaging was performed using an optical excitation source of four 30-W/810-nm laser diodes coupled to optical fibers and a Princeton Instruments/Acton PIXIS 1024BR camera (1024 x 1024 pixels) with a Schneider Optics 50-mm macro imaging lens, cooled to approximately -70°C. Time resolved photoluminescence (TRPL) measurements were performed using a 625-nm excitation source (200 fs pulses at 250 kHz) with an average power of 0.5 mW. All decays

were measured at 1100 nm. Single- or two- exponential fitting functions were used to fit the PL decay curves to derive the lifetime.

RESULTS and DISCUSSION

J-V Parameters

Figure 2 shows degradation in J-V parameters of the CIGS devices at different DH exposure times plotted using a Jump statistical software. Rows 1 through 4 represent samples encapsulated with glass, TPAT, TPT, and Tefzel, respectively. Different colors indicate different devices on the cell coupons encapsulated with a given backsheet for which the electrical performance was monitored. Devices encapsulated with glass and TPAT showed less degradation than the devices encapsulated with TPT and Tefzel, as the WVTR is the lowest for glass and TPAT. There is significantly less change in V_{oc} (~5% decrease) in the first 50 h, except for the cells encapsulated with Tefzel, while the J_{sc} dropped by ~10% in the initial 10 h of DH exposure for all of the coupons. The fill factor exhibited the greatest degradation amongst all the J-V parameters. The overall decrease in the efficiency during the first 50 h is attributed to the decrease in the fill factor and current density.

Series Resistance and Diode Ideality Factor

The changes in the series resistance (R_s) and ideality factor (A) are shown in the left and right columns respectively in Fig. 3, as obtained from modeling analysis of the light and dark J-V curves with a "CSU-curV-A" program. Samples encapsulated in glass show little or less change in both Rs and A. The sample encapsulated in TPAT show no change in Rs and A in the dark but a significant increase in Rs during illumination. Samples encapsulated in TPT show an increase in A. Samples encapsulated in Tefzel show a steep increase in Rs both in dark and in the light. The increase in the Rs is attributed to the degradation of ZnO, the front Ni/Al contact grid, and their interface contact.

Capacitance-Voltage Measurements

Figure 4 shows the changes in carrier concentrations (left column) and corresponding depletion width (right column) at zero bias extracted from C-V measurements at periodic intervals in the first 50 h of DH exposure. Figure 4(a) shows the carrier concentration decreased for devices encapsulated with glass, TPAT, and Tefzel. However, the carrier concentration increased in the first 10 h but decreased in the following 10 to 20 h for the devices

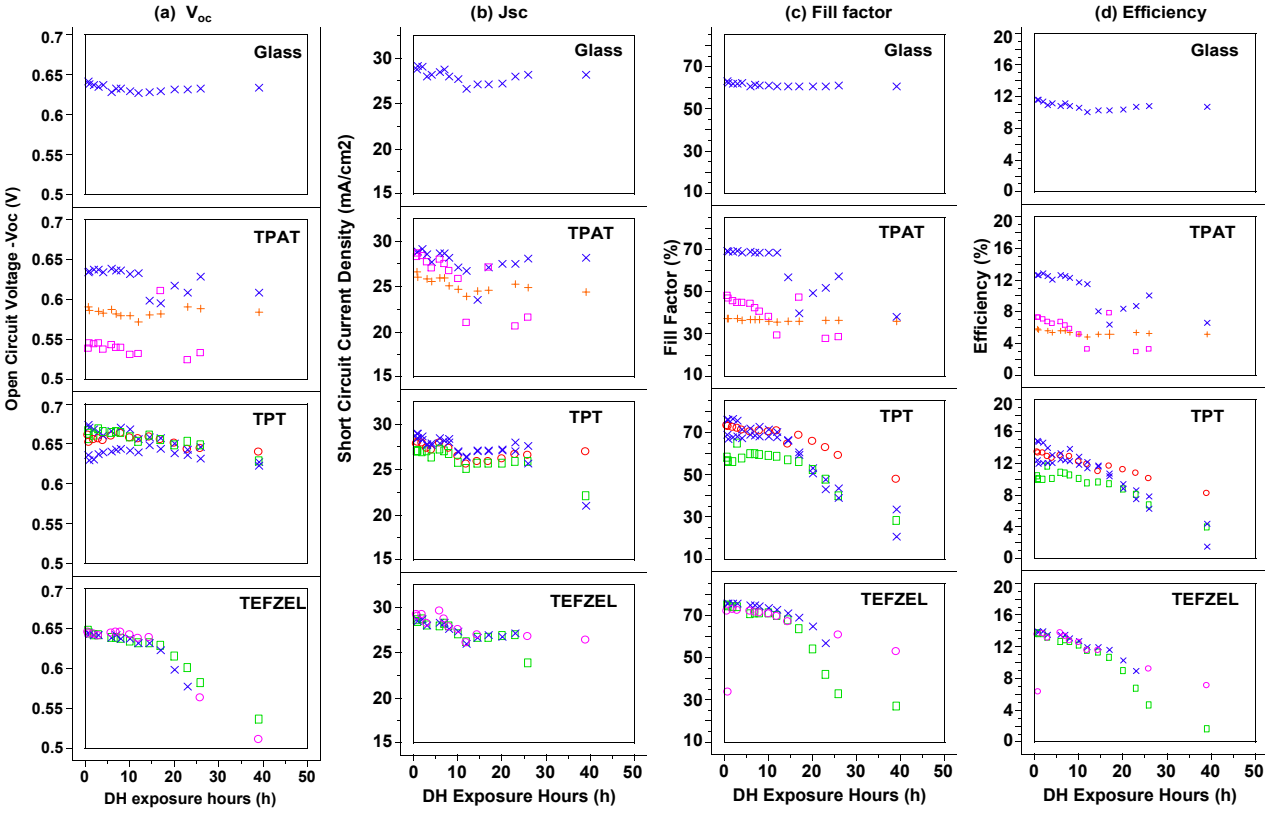

Figure 2 Degradation observed in J-V parameters (a) V_{oc}, (b) J_{sc}, (c) fill factor (FF), and (d) efficiency of CIGS devices as a function of DH exposure time for different encapsulation schemes (from top to bottom – Glass, TPAT, TPT and Tefzel, respectively in each column). Different symbols and colors indicate different devices in the same encapsulated sample set.

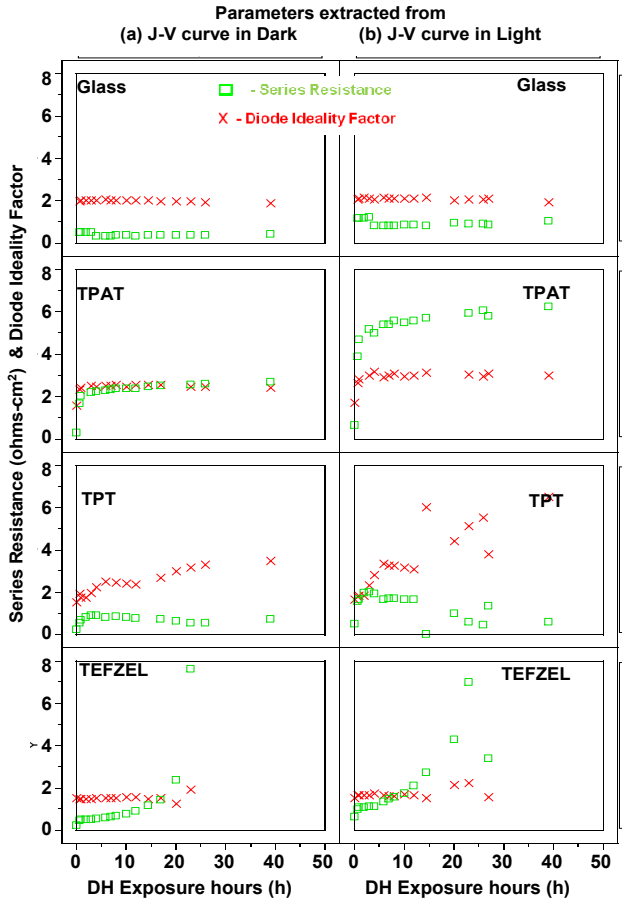

Figure 3 Change in series resistance (Rs) and diode ideality factor (A) of CIGS devices extracted from dark (left column) and light (right column) J-V curves and plotted as a function of DH exposure time. Open squares: Rs; symbol "x": A.

encapsulated with TPT as shown in Fig. 4 (3rd panel in left column). The corresponding trend in depletion width (W_d) change is shown in Fig. 4 (right column).

The decrease in carrier concentration and simultaneous increase in depletion width could be due to the reason that the mobile positive ions are driven into the bulk of the CIGS absorber layer by the built-in electric field; these positive ions could decrease the net acceptor density, eliminating the negatively charged vacancies and thus increasing the depletion width. Another possible explanation would be that as the ZnO layer degraded, the net donor concentration on the CdS side of the junction may change; this could require the W_d in the CIGS layer to adjust to maintain charge balance. Or that the traps that are filled by persistent photoconductivity are emptied by heat during exposure in the dark [5].

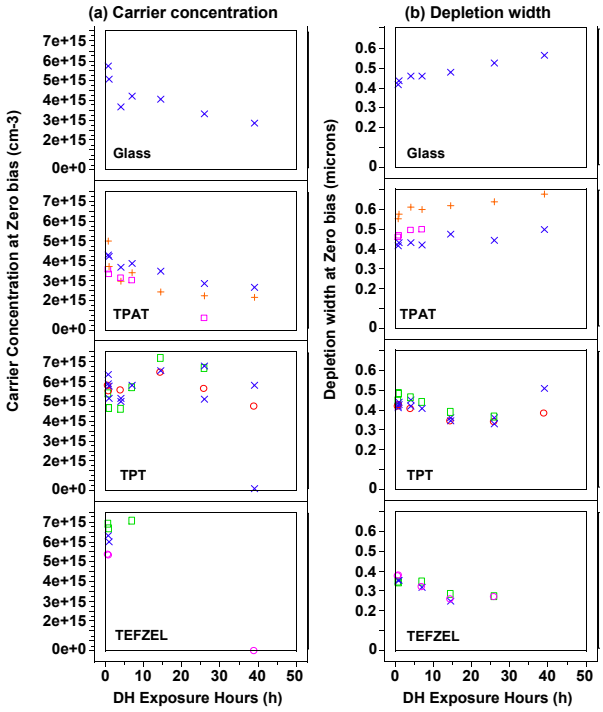

Figure 4 Change in carrier concentration (left column) and depletion width (right column) at zero bias at periodic intervals of DH exposure for CIGS devices encapsulated with different backsheets as indicated. Different symbols and colors indicate different devices on a cell coupon.

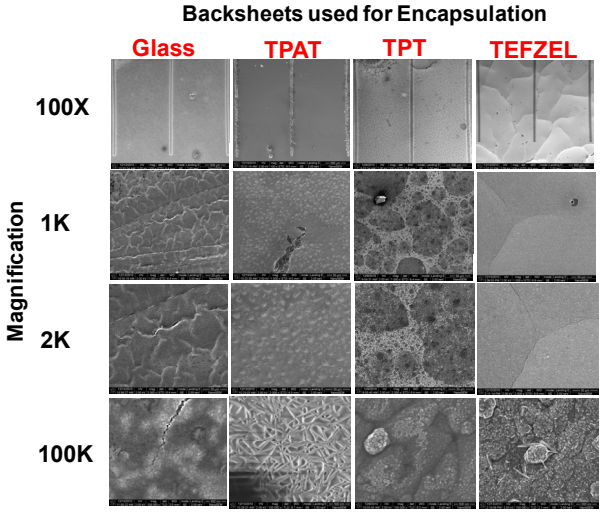

Figure 5 SEM images at different magnifications for surface morphology of the CIGS devices encapsulated with different backsheets after 700 h of DH exposure.

Morphology

Figure 5 shows the morphological changes on the devices after having been DH-exposed for 700 h and retrieved from the package. Devices in the glass encapsulation exhibited micro-cracks on the film surfaces, probably due to thermal stress by dry heat inside the package. The Tefzel encapsulated cells cracked through the entire film structure as visible from the back side of the glass, along with delamination between the substrate and Mo layer, obviously caused by the profuse amount of moisture. The devices encapsulated with TPAT and TPT exhibits sponge-like features, suggesting possible formation of $Zn(OH)_2$ on the AZO, further confirming our previous observations [6]. Corrosion of CIGS/Mo was observed over the regions in the isolation lines for the TPT-encapsulated devices (not shown), which exhibited micro-cracks and formation of nodules similar to that shown in the TPT and Tefzel SEM images at 100 X. The Ni/Al gridlines on the Tefzel- and glass-encapsulated devices exhibited corrosion, cracking, and peeling off from the surfaces, which would contributed to the increase of series resistance, Rs.

Surface Analysis

The formation of nodules and the composition of the AZO window layer were further investigated by XPS to analyze for the potential contaminants such as Ca, Sn, and mobile ions like Na from glass, which is beneficial to CIGS. For the amount of hydrogen in the interfacial layers, samples were analyzed using SIMS to see if we could relate this to the TCO degradation. The high-resolution XPS spectra taken at 5-eV pass energy of ZnO layer of the CIGS device shows the full-width half-maximum of the Zn-2p and O-1s peaks to be widened due to the chemical shift in the bonds between Zn and O, as a result of reaction of water with the ZnO surface. Oxygen 1s core level peaks were fitted with three individual peaks, which were identified as (1) binding energy range (529.9–530.7 eV) O-1s core level peak (O 1s pk1); (2) binding energy range (531.5–532.2 eV) for $Zn(OH)_2$ pk2; and (3) binding energy range (532.8–534 eV) for adsorbed water pk3 [7]. The calculated area under the individual peaks for each device retrieved from encapsulated package with different backsheets is shown in Figure 6. The area under the curve identified as the $Zn(OH)_2$ peak and the adsorbed water peak have strong correlation with the WVTR of the backsheet used for encapsulation, except for the glass-glass package. The device encapsulated in glass-glass was expected to show the least amount of chemical shifts of the ZnO peak, which was not the case, possibly due to leakage through the edge sealant around the Al frame edges. The device encapsulated with TPAT has the least amount of water adsorbed on the surface (0.75 and 4.18 atomic concentration %, (at. conc.%)), as it has the lowest WVTR, while the TPT-encapsulated devices show more water absorbed on the devices (~7 at. conc. %), and the Tefzel-encapsulated device shows the most (13.57 at. conc. %). The atomic concentration of the individual components for different encapsulations of the devices (not shown) are as follows: for the $Zn(OH)_2$ peak, the devices encapsulated with TPAT1 and TPT2 have the least amount (1.55 at. conc. %), while the glass, TPAT2, and TPT2 encapsulated devices have ~30 at. conc. % of $Zn(OH)_2$ on the surface, and the Tefzel-encapsulated device shows 43.42 at. conc. % of $Zn(OH)_2$.

The differences in the maximum intensity of hydrogen counts within the first 0.5 microns obtained from SIMS shown in Figure 7 could be due a thermal enhancement of the chemical reaction of water with the ZnO:Al layer forming $Zn(OH)_2$. SIMS data shows that the CIGS devices packaged with Tefzel had the highest hydrogen counts, as the WVTR of Tefzel was the highest amongst all the packages. This can be well-correlated with the component of $Zn(OH)_2$ peak of the curve fitted oxygen core level from the XPS data.

Time Resolved Photo Luminescence

Minority carrier lifetime of CIGS and CIGS/CdS *absorber films* is of the order of ~250 ns. But when ZnO is deposited the lifetime decreases by two orders of magnitude,

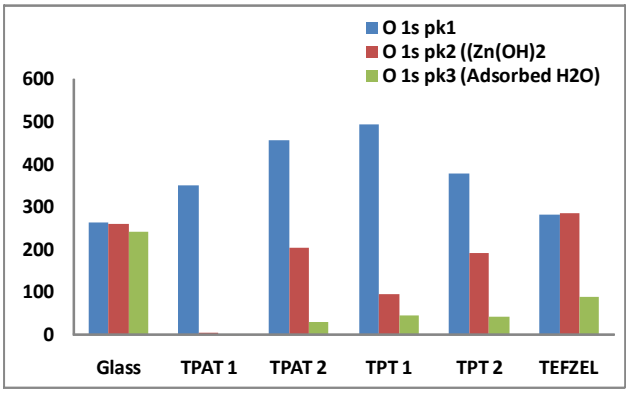

Figure 6 Area under individual XPS peaks of O 1s core level identified as O 1s core, $Zn(OH)_2$, and adsorbed H_2O for CIGS devices encapsulated in different backsheets after 700-h DH exposure.

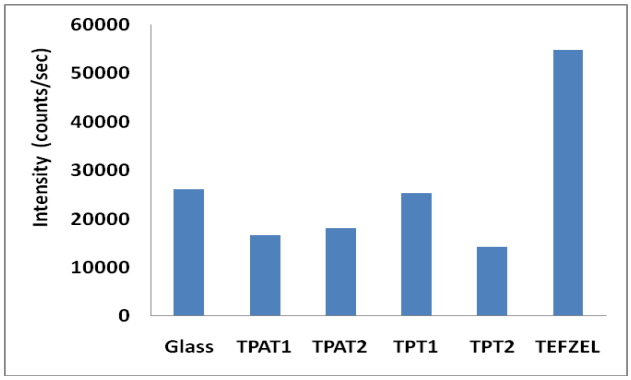

Figure 7 SIMS intensity counts of the element hydrogen in CIGS devices encapsulated with different backsheets after 700 h of DH exposure.

because of the carrier kinetics due to the electric field formed in the junction and not because of recombination [8-10]. Table 1 shows the TRPL-derived values of the fast recombination rate (τ_1) obtained for the devices that showed dismal electrical performance after 700-h DH exposure. Minority carrier lifetimes for all CIGS devices are on the order of ~8 ns, which is relatively long compared to life time of 20% efficient devices which is of the order of subnano seconds. Devices encapsulated with TPAT and Tefzel had shorter lifetimes at ~3.6 and ~1.85 ns, respectively. The reason for the shorter lifetimes for devices encapsulated with Tefzel could be the high WVTR, and that with TPAT could be that the package had wrinkles at the corners that could have caused the moisture seepage and degradation. The ~8 ns lifetimes of these devices as opposed to the shorter lifetimes (<300 ps) of freshly prepared CIGS PV devices is indicative that the CIGS film quality has remained "relatively good" after exposure to DH for ~700 h, while collection of the carriers is affected by degradation of the ZnO, This is further confirmed by the photoluminescence images taken.

Table 1 Lifetime of CIGS devices extracted from TRPL measurements after 700 h of DH exposure.

Device ID	Backsheet	Lifetime τ_1 (ns)
M3133-12	N/A, stored in ambient	6.25
M3147-22	Glass	8
M3147-12	TPAT1	8.56
M3147-13	TPAT2	3.64
M3147-11	TPT1	8.87
M3147-21	TPT2	7.9
M3147-23	Tefzel	1.85

After DH exposure, the CIGS devices were retrieved from the individual package for investigation using photoluminescence (PL). Figure 8 shows the PL images taken before and after 700 h of DH exposure of glass-, TPAT-, TPT-, and Tefzel-encapsulated CIGS coupons, respectively from top to bottom. Before DH exposure, the bright intensity of the individual devices shows that the devices had no shunts or other defects, such as weak diodes. After DH exposure, glass-encapsulated devices 1, 2, and 4 (counting from right) were degraded. For the device encapsulated in TPAT, there was a bright band with a strong intensity in between dark bands. For the TPT-encapsulated devices, there were visible small-to-medium shunts corresponding to dark spots seen at the bottom of the two devices at the extreme left, while complete degradation was observed for devices encapsulated with Tefzel that has the highest WVTR.

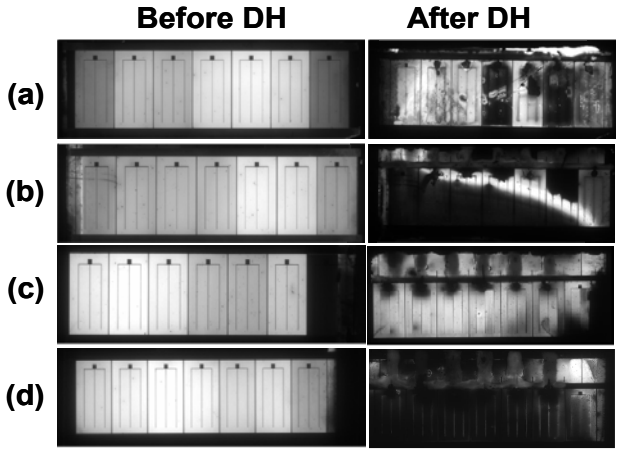

Figure 8 PL of CIGS devices retrieved from a) glass, b) TPAT, c) TPT, and d) Tefzel encapsulation after 700-h DH exposure.

The bright intensity in some of the devices in all of the cell coupons indicates that CIGS absorber might be still good after DH exposure, even though the device itself has lost its electrical performance due to the fact that carriers are not collected efficiently as a result of degradation of TCO or the CdS buffer layer. In order to confirm this hypothesis, the CIGS device encapsulated in TPAT was etched to remove the Ni/Al contact grids, bilayer ZnO, and CdS layer. The etch-cleaned CIGS film was reprocessed with new layers of CdS, *i*-ZnO, ZnO:Al, and Ni/Al grids. The devices were isolated with manual scribes and J-V re-measured. Table 2 compares the J-V parameters for the device M3147-12-3 for different DH exposure hours. The severe shunting seen after encapsulation has disappeared after repeated DH exposures. After re-fabrication even though there is a drop in Voc, the FF and J_{sc} have improved with respect to that for the 784 h DH-exposed device, indicating the decrease in the J_{sc} was primarily due to hydrolysis of the TCO window layer and Ni/Al contact grids, both caused increase in series resistance, Rs.

Table 2 Comparison of the J-V parameters at various exposure times and after re-fabrication of the new TCO layer.

DH Exposure Time (h)	V_{oc} (V)	J_{sc} (mA/cm^2)	FF (%)	Efficiency (%)
0	0.69	32.8	78	17.7
1	0.64	28.1	58	10.4
784	0.65	19.9	59	7.6
N/A, after re-fabrication	0.56	28.4	60.9	9.68

The current-density vs. voltage curves before and after the etch are plotted together in Fig. 9 to illustrate that the degradation of the TCO and the contacts and the increase in shunt conductance are the main driving factors that reduced the fill factor and, in turn, the efficiency. The slopes of the J-V curves of the re-fabricated device are steep and similar to that of the device at its initial state, indicating that the degradation and the decrease in the J_{sc} can be attributed in part to the changes in the chemical composition of the ZnO window layer.

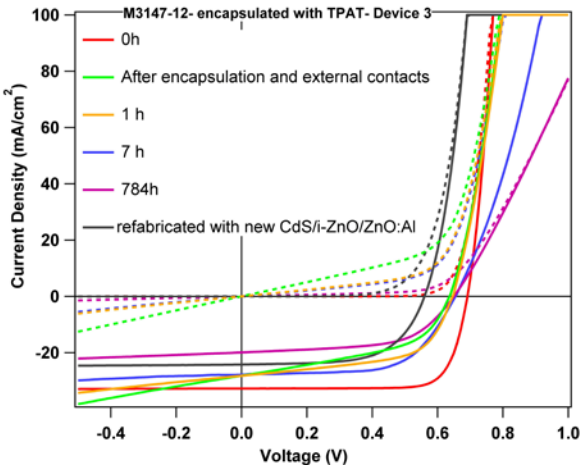

Figure 9 J-V curves of M3147-12 device #3 encapsulated in TPAT before and after etch and re-fabrication after 784 h of DH exposure.

PL image in Fig. 10 shows that the re-fabricated devices #3, 4 and 5 have bright intensity, indicating the devices has been restored by the new buffer and window layer.

Fig. 10. PL image of M3147-12 re-fabricated with new layers of CdS, *i*-ZnO, ZnO:Al and Ni/Al grids.

CONCLUSIONS

This study investigated and characterized the failure mechanisms involved in the degradation of CIGS devices by DH exposure by using various electrical, optical, and morphological techniques. The results from all characterizations point to the fact that the CIGS degradation mechanism induced by DH is mainly due to the degradation of ZnO and metal contact grids as well, resulting in an increase in series resistance and shunt conductance, and consequent decrease in fill factor and cell efficiency.

ACKNOWLEDGEMENTS

We thank Ingrid Repins, Steve Glynn, and Clay DeHart for fabrication of the CIGS devices. This work was performed at the National Center for Photovoltaics and supported by the U.S. Department of Energy under Contract No. DE-AC36-08-GO28308 with the National Renewable Energy Laboratory.

REFERENCES

[1] J. Wennerberg, J. Kessler, M. Bodegard and L. Stolt, "Damp Heat Testing of High Performance CIGS Thin Film Solar Cells," *Proc. 2nd World Conference and Exhibition on Photovoltaic Energy Conversion*, July 6-10, 1998, Vienna, Austria, pp. 1161-1164.

[2] J. Klaer, R. Klenk, A. Boden, A. Neisser, C. Kaufmann, R. Scheer, H.-W. Schock, "Damp Heat Stability of Chalcopyrite Mini-Modules," *Proc. 31st IEEE PVSC*, 2005, pp. 336-339.

[3] R. Sundaramoorthy, I.L. Repins, F.J. Pern, D. Albin, J. Li, M. Contreras, T. Gessert, T. Gennet, J. Perkins, D. Ginley, and C. DeHart, "Comparison of Polycrystalline ZnO:Al and Amorphous InZnO as A Conductive Layer for CIGS PV Solar Cells," *Proc. 34th IEEE PVSC*, Philadelphia, PA, June 7-12, 2009, pp. 001576 - 001581.

[4] R. Sundaramoorthy, F.J. Pern and T. Gessert. "Preliminary Damp-Heat Stability Studies of Encapsulated CIGS Solar Cells," *Proc SPIE Conference on Reliability of Photovoltaic Cells, Modules, Components and Systems*, Aug. 1-5, 2010, San Diego, CA.

[5] M. Igalson, A. Urbaniak, A. Krysztopa, Y. Aida, R. Caballero, M. Edoff, "Sun Bandgap Photoconductivity and Photocapacitance in CIGS Thin Films and Devices, "Thin Solid Films. In press, 2011

[6] F.J. Pern, B. To, S.H. Glick, R. Sundaramoorthy, C. DeHart, S. Glynn, C. Perkins, L. Mansfield, and T. Gessert, "Variations in Damp Heat-Induced Degradation Behavior of Sputtered ZnO Window Layer for CIGS Solar Cells," Proc. SPIE PV Conference #7773 "Reliability of Photovoltaic Cells, Modules, Components, and Systems III", 8/1-5/2010 San Diego, CA.

[7] W. Eisele, A. Ennaoui, P. Schubert-Bischoff, M. Giersig, C. Pettenkofer, J. Krauser, M. Lux-Steiner, S. Zweigart, and F. Karg, "XPS, TEM and NRA Investigations of $Zn(Se,OH)/Zn(OH)_2$ Films on $Cu(In,Ga)(S,Se)_2$ Substrates for Highly Efficient Solar Cells," *Solar Energy Materials and Solar* Cells **75,** 2003, pp.17-23.

[8] W.K. Metzger, I.L. Repins, and M.A. Contreras, "Long Lifetimes in High-Efficiency $Cu(In,Ga)Se_2$ Solar Cells", *Applied Physics Letters* **93**, 2008, pp. 022110

[9] I.L. Repins, W.K. Metzger, C.L. Perkins, Jian V. Li, and M.A. Contreras, "Correlation between Measured Lifetime and CIGS Device Performance," *IEEE transactions on Electron devices*, **57**, 2010, pp. 2957-2963.

[10] B.M. Keyes, P. Dippo, W. Metzger, J. AbuSharma, and R. Noufi, "CIGS Thin Film Evolution During Growth - A Photoluminescence Study," Proc. *29th IEEE-PVSC*, 2002, pp. 511 - 514.